# Magnetite/graphene composites: microwave irradiation synthesis and enhanced cycling and rate performances for lithium ion batteries†

**Ming Zhang, Danni Lei, Xiaoming Yin, Libao Chen,* Qiuhong Li, Yanguo Wang and Taihong Wang***

*Received 9th March 2010, Accepted 1st April 2010*
*First published as an Advance Article on the web 3rd June 2010*
**DOI: 10.1039/c0jm00638f**



By employing microwave irradiation as a heat source, magnetite/graphene composites were synthesized by depositing $Fe^{3+}$ in the interspaces of graphene sheets. The $Fe_3O_4$ nanoparticles were dispersed on graphene sheets. As anode materials for lithium ion batteries, they showed high reversible capacities, as well as significantly enhanced cycling performances (about 650 mA h $g^{-1}$ after 50 cycles) and high rate capabilities (350 mA h $g^{-1}$ at 5 C). The enhancement could be attributed to graphene sheets, which served as electron conductors and buffers. Our results opened a new doorway for the application of graphene sheets to prepare anode materials of lithium ion batteries with superior performances.

## Introduction

As a kind of rechargeable batteries, lithium ion batteries have attracted considerable attention due to their higher voltage, higher specific energy, and longer cycle life compared with conventional batteries,[1–6] such as lead–acid,[7] Ni–Cd,[8] Ni–MH,[9] and Ag–Zn[10] batteries. Although they have the highest energy density available from existing rechargeable battery techniques, their performances still lie behind the demands of the consumer, especially their rate capability.

Since transition metal oxides were first reported as active anode materials for lithium ion batteries, they have attracted much attention because of their high specific capacities.[11–13] In particular, magnetite is an attractive anode material for next generation lithium ion batteries due to its high capacity, eco-friendliness, natural abundance, and high electronic conductivity.[14] However, their application in practical lithium ion batteries was hindered owing to their low rate performance arising from kinetic limitations and poor cycling stability resulting from large volume expansion occurring during cycling.[15] Various methods have been tried to improve its cycling performance and rate capability, including coating carbon layers[13,16] and decreasing the size of particles.[15] Nevertheless, there were few reports that discussed the possibility of improving the performance of $Fe_3O_4$ as anode materials for lithium ion batteries with the help of graphene sheets (GSs). In this work, to modify the magnetite, $Fe_3O_4$/graphene composites (MGCs) were synthesized.

Graphene is a two-dimensional aromatic monolayer of carbon atoms. Actually, it is the building unit of graphite. Recent studies demonstrated that graphene exhibited unique electronic behaviors, such as its room temperature quantum Hall effect,[17] and its mimic massless transportation properties,[18] resulting in a super high conductance. Moreover, it has been proposed that lithium ions could be adsorbed on both sides of graphene sheets, which leads to two layers of lithium for each graphene sheet, with a theoretical capacity of 744 mA h $g^{-1}$ through the formation of $Li_2C_6$.[19,20] Combined with the merits of magnetite and graphene, the electrochemical performances were supposed to be greatly enhanced.

Although magnetite/graphene composites could be synthesized by some methods as reported in the literature,[21–23] those methods were either tedious or in need of organic solutions and expensive raw materials. Recently, microwave-assisted methods have been widely used to synthesize nanomaterials, as they offer great advantages, including faster synthesis and higher energy efficiency, as compared with conventional methods.[24,25] Except the rapid transfer of microwave energy to thermal energy in polar solution (such as water), the penetration properties of microwave electromagnetic irradiation through solutions should result in a uniform heating for the reaction solution, giving uniform nucleation and growth rates, as compared with thermal convection. To the best of our knowledge, it was the first time that MGCs were synthesized by a microwave irradiation method with inexpensive raw materials.

In this study, $Fe^{3+}$ were deposited by urea with uniform nucleation and growth rates by a microwave irradiation process. At same time, graphene oxide (GO) was reduced by ascorbic acid (AA). As a result, $Fe_3O_4$ nanoparticles were interspersed on GSs with some interspaces between them. Electrochemical measurements showed that the composite anode has a high initial discharge capacity (1320 mA h $g^{-1}$) and a reversible discharging capacity of 650 mA h $g^{-1}$ over 50 cycles. Moreover, the discharge capacity of MGCs was still 350 mA h $g^{-1}$, in despite of a high rate of 5 C (discharge/charge of all active materials within 12 min), which was better than commercial $Fe_3O_4$ nanoparticles (CMPs) and carbon coated magnetite reported by previous papers.[13,16] All the results showed that modifying the magnetite particles by GSs was an effective strategy to enhance the properties of magnetite nanoparticles as anode materials of lithium ion batteries.

*Key Laboratory for Micro-Nano Optoelectronic Devices of Ministry of Education and State Key Laboratory for Chemo/Biosensing and Chemometrics, Hunan University, Changsha, 410082, China. E-mail: thwang@hnu.cn; lbchen@hnu.edu.cn*

† Electronic supplementary information (ESI) available: Raman and TG characterization of magnetite/graphene composites.

 

## Experimental

Graphite powders were purchased from Alfa Aesar China (Tianjin) Co. Ltd. Iron nitrate nonahydrate ($Fe(NO_3)_3 \cdot 9H_2O$), ascorbic acid (AA, $C_6H_8O_6$) and urea ($CO(NH_2)_2$) were purchased from Sinopharm Chemical Resgent Co. Ltd (Shanghai, China). All other chemicals were of analytical grade and used as received without any purification process. The water was Millipore Milli-Q grade with a resistivity larger than 18 MΩ $cm^{-1}$.

GO was prepared from graphite powders according to a modified Hummers' method.[26] Exfoliation was carried out by sonicating the GO dispersion (2 mg $mL^{-1}$) under ambient condition for 2 h. Then, we prepared a mixture of GO, $Fe(NO_3)_3$, urea and ascorbic acid with concentrations of 1.5 mg $mL^{-1}$, 0.027 M, 0.25 M and 0.057 M, respectively. Next, the mixture was refluxed under ambient conditions for 1 h with a microwave heater. Before being oven-dried overnight at 353 K, the products were purified by washing repeatedly with deionized water and isolated by centrifugation. Finally, MGCs were obtained by treating above products in Ar atmosphere at 873 K for 8 h with a rate of 10 K $min^{-1}$. The synthesis processes of GSs were similar to that of MGCs except the urea and iron nitrate nonahydrate.

The composites were characterized by powder X-ray diffraction (XRD) on a SIEMENS D5000 X-ray diffractometer with Cu Kα irradiation ($\lambda$ = 0.15406 nm). The microstructure and morphology of the composites were analyzed by a Hitachi S4800 scanning electron microscope (SEM), and a JEOL-2010 transmission electron microscope (TEM) at a 200 kV accelerating voltage. To analyze the elements of MGCs, energy dispersive X-ray (EDX) analysis was also carried out. Thermogravimetric analysis (TGA) data were achieved on a Netzsch STA449C. Raman spectra were obtained using a confocal microprobe Raman system (LabRam-010, 632 nm as excitation source).

The electrochemical properties of the products were measured using CR2016-type coin cells. In a process of fabricating the lithium ion batteries, electrodes were prepared by compressing a mixture of active materials (including the MGCS, GSs or CMPs) (80 wt%), carbon black (10 wt%) and polyvinylidene fluoride (PVDF, 10 wt%) on pure copper foils. The mass of active materials on each anode was *ca.* 0.6 mg. A Celgard 2400 microporous polypropylene membrane was used as a separator. The electrolyte consists of a solution of 1 M $LiPF_6$ in ethylene carbonate/dimethyl carbonate/diethyl carbonate (1 : 1 : 1, in wt%). Pure lithium foils were used as counter electrodes. These cells were assembled in an argon-filled glovebox with water and oxygen contents less than 1 ppm. The discharge and charge measurements were carried on an Arbin BT2000 system with the cut off potentials being 0 V for discharge and 3 V for charge.

## Results and discussion

MGCs were prepared by simultaneously chemical depositing iron ions and reducing the GO. This approach, schematically illustrated in Scheme 1, started with the dispersion of the GO in deionized water. Secondly, $Fe^{3+}$ were captured by hydroxyls (possible carboxyls or epoxies) on the GO by coordination.[22] Thirdly, mixtures (sample A), containing Fe, O, H elements and GSs, were gained by treating iron ions coordinated with GO and aqueous urea solution with microwave irradiation. Because the GO could absorb microwave irradiation,[27] the temperature of the solution near the GO was higher than that of other regions. Therefore, urea molecules could be hydrolyzed easily in this region, accelerating the deposition of $Fe^{3+}$ on the surface of GO. Furthermore, microwave heating methods could address the problem of heating inhomogeneity, resulting in uniform nucleation and growth rates. Thus the nanoparticles of sample A were very small. Finally, partial $Fe^{3+}$ was reduced and the MGCs were obtained by processing sample A in Ar at high temperature.

Compared with conventional methods, microwave synthesis has the advantages of very short reaction time and production of small particles with narrow size distribution.[28] The SEM image

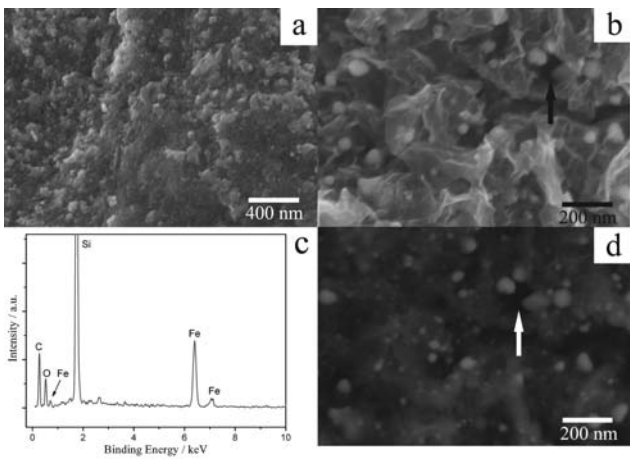


**Fig. 1** SE SEM images of sample A (a) and MGCs (b) and EDX (c) and a BSE SEM image (d) of the MGCs.

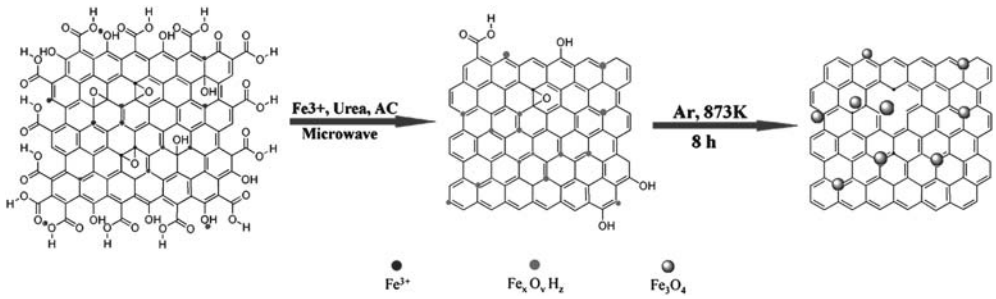


**Scheme 1** A synthetic scheme of magnetite particles dispersed on GSs by a microwave irradiation method.

of sample A is shown in Fig. 1(a). As expected, sample A is composed of many small nanoparticles. Fig. 1(b) shows a secondary electron (SE) SEM image of MGCs. Both GSs and $Fe_3O_4$ nanoparticles are visible. The diameter of the $Fe_3O_4$ nanoparticles is about 20–70 nm, larger than that of the particles in sample A. Therefore, high-temperature processing results in the increase of the diameters of the particles. Further, the $Fe_3O_4$ nanoparticles are connected together by GSs, constructing graphene intercalation compounds. Besides, the interspaces among them are also observed. A back-scattering electron (BSE) image (containing 30% information of BSE) of the same area of MGCs is shown in Fig. 1(d). The two arrows in Fig. 1(b) and (d) mark the same region of the sample. It is well known that the BSE image provides information on the composition of the sample.[29] In Fig. 1(d), the bright areas represent the areas of Fe and O and the dark areas are C. By comparison of Fig. 1(b) and (d), it could be concluded that $Fe_3O_4$ particles disperse on GSs and there are some interspaces among them. EDX characterization of MGCs is presented in Fig. 1(c). The results show the presence of C, O, Fe and Si, arising from MGCs and the silicon substrate.

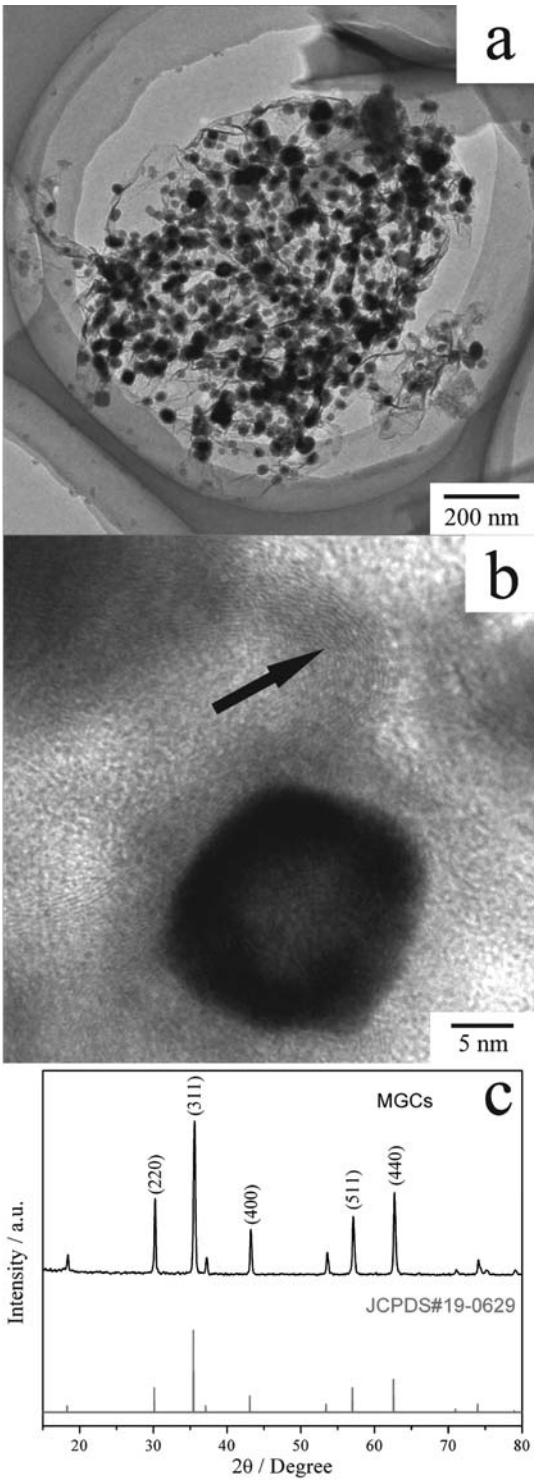


**Fig. 2** Low (a) and high (b) magnification TEM images of MGCs and XRD patterns (c) of MGCs. The arrow in panel (b) marks bent GSs.

TEM images of MGCs are show in Fig. 2. The low-magnification image (Fig. 2(a)) shows that the sample consists of GSs and magnetite nanoparticles with a diameter of 20–70 nm, indicating that dispersed magnetite has been achieved with the present approach. The morphology of a single nanoparticle is shown in Fig. 3b. The particle is hollow with a diameter of about 20 nm. This structure is favorable to release the strains of $Li^+$ insertion/extraction, resulting in a good cycling performance.[30] Moreover, a bundle of curving sheets is also observed, which is caused by the bending of the graphene sheets at high temperature owing to the strain. The bent GSs, serving as buffers, are also propitious to improve the cycling performance of $Fe_3O_4$ nanoparticles.

The crystal structure of the final products was characterized and the results are presented in Fig. 2(c). The upper curve in Fig. 2(c) is the XRD patterns of MGCs and the lower one indicates the JCPDS date (JCPDS File Card No. 19-0629). The diffraction patterns and relative intensities of all diffraction peaks matched well with those of the magnetite. It could be concluded that the $Fe_3O_4$ particles were prepared by partial reduction of $Fe^{3+}$ to $Fe^{2+}$. The gain of weight in the TG experiment also demonstrated the presence of $Fe^{2+}$ in MGCs (shown in fig. S1 of the ESI†). No obvious XRD peaks corresponding to graphite are found in the XRD pattern, indicating that GSs are not well crystallized and there are some biggish spaces between GSs. In the Raman spectra of MGCs (shown in fig. S2 of the ESI†), the intensity ratio of the D to G band ($I_D/I_G$) is calculated as 1.32 for the samples, further reflecting the relative disorder and a low graphitization degree.[31]

The electrochemical properties of MGCs with respect to $Li^+$ insertion/extraction were investigated and the corresponding cyclic voltammograms (CVs) are shown in Fig. 3(a). In the first cycle, a peak in the cathodic processing is observed at about 0.4 V, which could be attributed to the reduction of $Fe^{3+}$ and the irreversible reaction with the electrolyte.[32] The anodic peak at 1.8 V corresponds to the reversible oxidation of $Fe^0$.[32] During the anodic process, both the peak current and the integrated area of the anodic peak are changeless, indicating no capacity loss during the charging process. Fig. 3(b) shows the CVs of CMPs. The potential of their cathodic and anodic peaks are similar to that of MGCs. But the peak current and the integrated area of their anodic peak quickly decreased, suggesting capacity loss during the $Li^+$ extraction. The above results indicate that MGCs synthesized by our method show an improved cycling performance. The charge/discharge curves of MGCs and CMPs for the

 

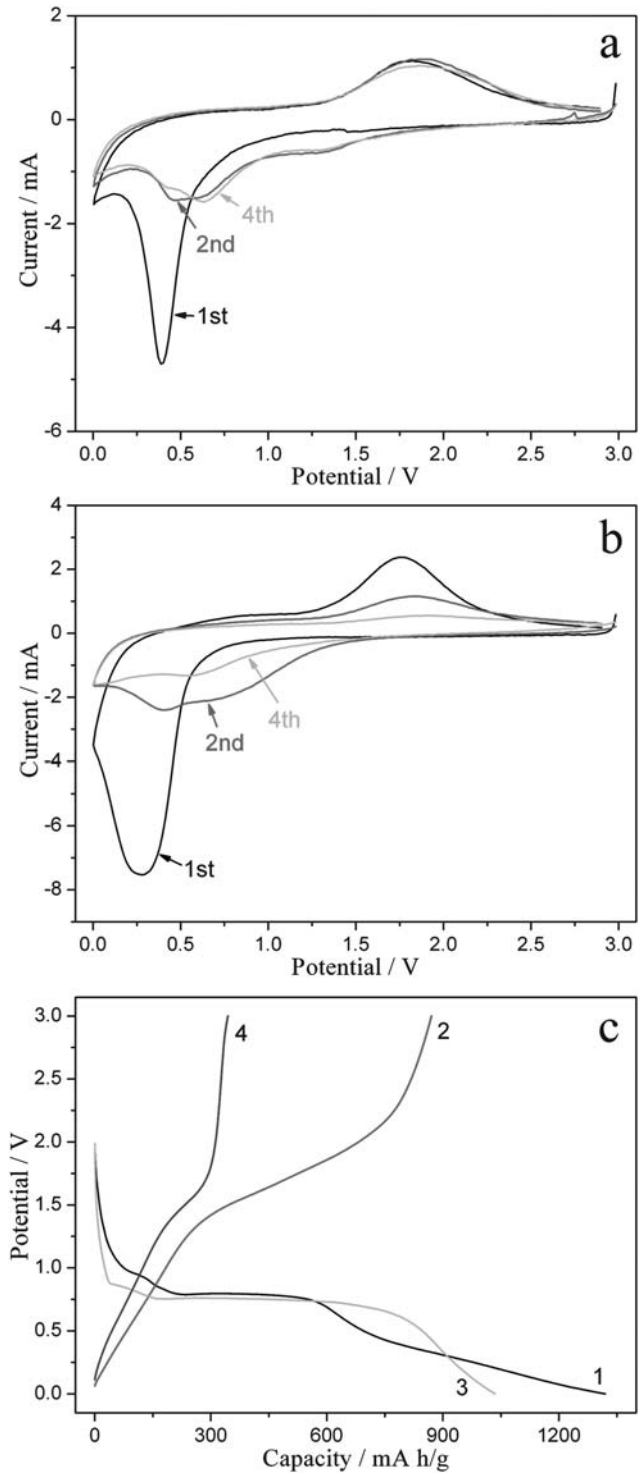


**Fig. 3** Cycic voltammograms of MGCs (a) and CMPs (b), the scan speed is 0.5 mV $s^{-1}$. Panel (c) shows the first discharge/charge profiles of MGCs (1, 2) and CMPs (3, 4) cycled at a rate of C/10.

first cycle are shown in Fig. 3c. Their obvious potential plateaus during charge/discharge processing are almost the same and located at 0.8/1.6 V. Due to hysteresis in the CV technique, the voltage value of the cathodic peak is shifted to a negative direction, and the anodic peak is positively shifted compared to the voltages of the charge/discharge plateaus.[32] These results are consistent with previous reports.[16,32] The discharge capacity of MGCs in the first cycle is 1320 mA h $g^{-1}$, which is a little larger than that of CMPs (1030 mA h $g^{-1}$). However, the charge capacity of MGCs (870 mA h $g^{-1}$) is obviously higher than that of CMPs (344 mA h $g^{-1}$), indicating a larger reversible specific capacity of MGCs.

It is well known that anode materials based on carbon materials exhibit a good cycling performance.[16] Hence, to study the effect of GSs on the cycling performance of the magnetite as anode materials for lithium ion batteries, we employed MGCs to prepare lithium ion batteries and investigated their cycling performance. The electrochemical properties of GSs and CMPs were also investigated for comparison. Fig. 4 compares the cycling behavior of MGCs and CMPs. The initial discharge capacities of MGCs and CMPs are 1320 and 1030 mA h $g^{-1}$ at a rate of C/10, which are higher than the theoretical capacity of $Fe_3O_4$. The extra capacity excess over the theoretical value could be attributed to the decomposition of the electrolyte and the formation of the solid electrolyte interphase (SEI) layer in the first cycle.[32] The capacities of CMPs fade to 130 mA h $g^{-1}$ at the fifth cycle and then gradually decrease to 70 mA h $g^{-1}$ (curve (D) of Fig. 4(a)). The capacities of MGCs also decrease to about 860 mA h $g^{-1}$ at the fifth cycle, but their capacity remains at 650 mA h $g^{-1}$ even after 50 discharge/charge cycles (curve (C) of

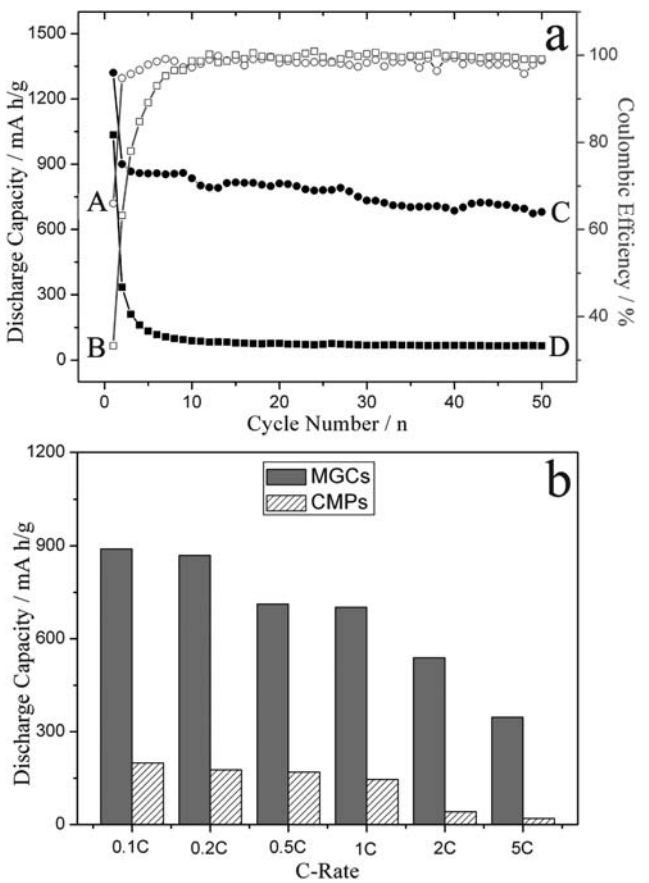


**Fig. 4** (a) A plot of the coulombic efficiencies of the MGCs (A) and CMPs (B) *vs.* cycle number and the electrochemical cycling performances of the MGCs (C), and CMPs (D) at a charge/discharge rate of C/10. (b) The rate performance of MGCs and CMPs.

Fig. 4(a)), which is almost 1.7 times that of the theoretical specific capacity of currently used graphite (372 mA h $g^{-1}$), and 9 times of that of CMPs. Moreover, compared with the anode materials of carbon coated $Fe_3O_4$ reported in the literature,[13,16,32,33] a higher cycling performance is achieved by modifying the magnetite with GSs. With the presence of GSs, not only the cycling performance of the magnetite as anode materials is improved, but its coulombic efficiency is also enhanced. The coulombic efficiencies of MGCs and CMPs are illustrated in curves (A) and (B) of Fig. 4(a), respectively. It can be found that the coulombic efficiency of the MGCs is the highest before the tenth cycle. There is no obvious difference among their coulombic efficiencies after the eleventh cycle.

Although the magnetite is a kind of transition metal oxide with a high electronic conductivity,[14] its conductance is still not sufficient for the demands of charge/discharge with high rates. It had been demonstrated that the rate capability of transition metal oxides was increased by carbon-coatings.[16] Therefore, the rate capability of MGCs was characterized and the results are presented in Fig. 4(b). As expected, the reversible capacities of the MGCs decrease slowly with increasing rate from 0.1 C to 5 C compared with CMPs. At a high rate of 5 C, the reversible capacities of the MGCs remain at 350 mA h $g^{-1}$, whereas CMPs have nearly no capacity under this condition. Table 1 shows a comparison of the discharge capacities at different rates between the anode materials reported before and in this work. It can be seen that the capacities of the MGCs were higher than other materials at the same discharge rate. The results indicate that modifying $Fe_3O_4$ nanoparticles with GSs are an effective way to improve both the cycling and the rate performance of $Fe_3O_4$-based anode materials.

**Table 1** The rate capacities of $Fe_3O_4$/C composites reported before and in this work (mA h $g^{-1}$)

| | Discharge rate | | | | | | |
|---|---|---|---|---|---|---|---|
| Materials | 0.1 C | 0.2 C | 0.5 C | 1 C | 2 C | 5 C | Ref. |
| $Fe_3O_4$/C | 640 | — | 430 | 350 | 280 | 170 | [13] |
| $Fe_3O_4$/C | — | 730 | 580 | 510 | 380 | 190 | [16] |
| MGCs | 890 | 870 | 710 | 700 | 540 | 350 | This work |

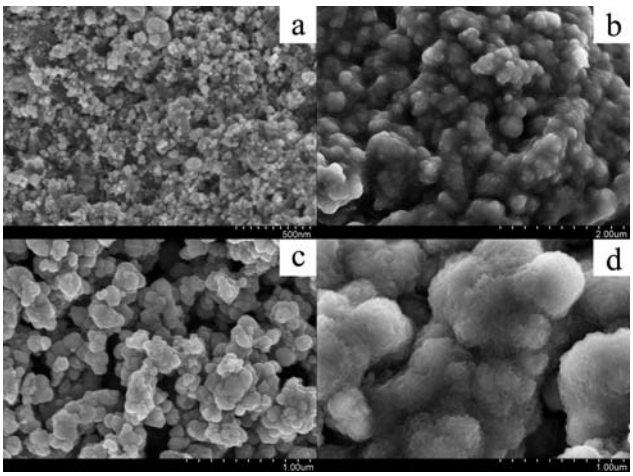


**Fig. 5** SEM images of the MGCs (a) and CMPs (c) as anode materials on copper foils and SEM images of the MGCs (b) and CMPs (d) in a fully lithiated state after 50 cycles.

The above results demonstrate that MGCs are excellent anode materials for lithium ion batteries. However, the essential reason is not clear. In order to better understand the effects of GSs on the electrochemical properties of $Fe_3O_4$ nanoparticles, we examined their morphology change after electrochemical cycles. They were investigated on the copper foils by SEM. Because the MGCs and CMPs on copper foils were mixed with carbon black and PVDF, their morphologies were changed a little. Fig. 5(a) and (b) shows the SEM photos of MGCs before (a) and after (b) 50 cycles. The SEM photos of CMPs before (c) and after 50 cycles (d) are also shown in Fig. 5. Nearly all the $Fe_3O_4$ nanoparticles are unbroken on the battery electrodes (Fig. 5(b)) and their SEI films are dense and slick, indicating that the composites are stable and strong enough to withstand the casting

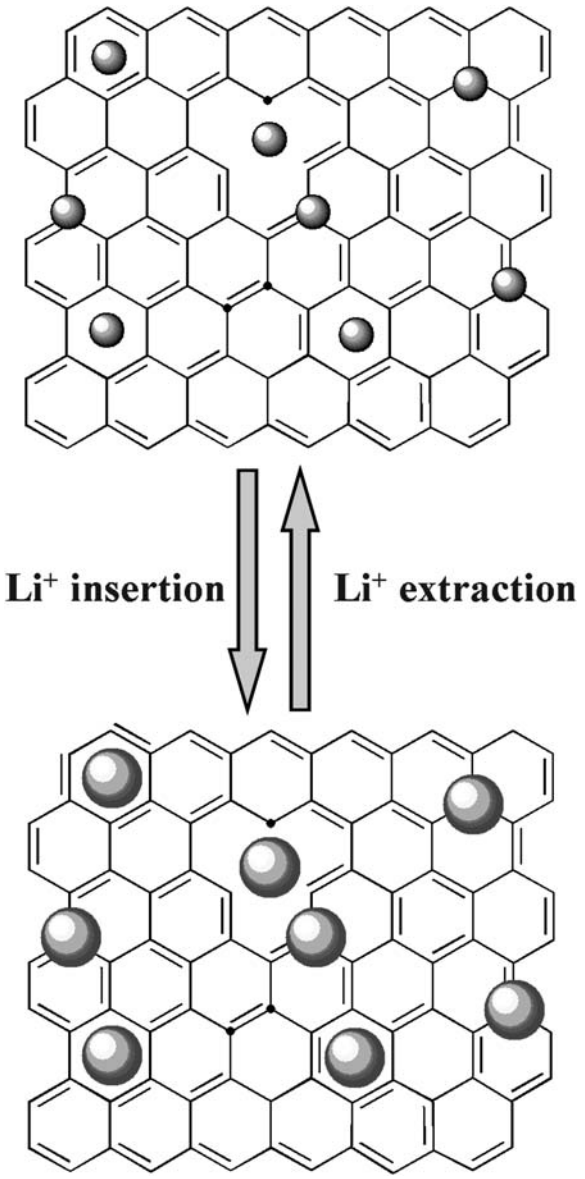


**Scheme 2** A schematic illustration of the role of the interspaces among $Fe_3O_4$ nanoparticles in improving their performances.

 

and pressing processes necessary for battery fabrication. On the other hand, a change in morphology is obvious for CMPs (Fig. 5(d)). The CMPs are coated by loose and rough films, which should dissolve faster than dense layers. Hence, the SEI films on MGCs are more stable than those on CMPs. The results indicate that the GSs can effectively protect the active materials.

Previous results showed that the cycling performance and rate capability of MGCs were better than those of CMPs. Considering the difference between MGCs and CMPs, a possible reason why MGCs show superior performances is explained as follows, as shown in Scheme 2. By microwave irradiation, $Fe^{3+}$ ions were deposited *in situ* in the interspaces of GSs or on them.[22] At same time, GO was reduced by AA. After processed at high temperature, $Fe_3O_4$ nanoparticles were sprinkled on GSs and were connected by the GSs. As have been proved by SEM, TEM and XRD, there were some interspaces between the $Fe_3O_4$ nanoparticles. The interspaces were propitious to release the strains arising from $Li^+$ insertion/extraction.[34] In the MGCs, the GSs played the two roles of conductors and buffers. Namely, they not only served as an electron conductive network, but also released the strains of $Li^+$ insertion/extraction.[34] However, CMPs joined together. There were few interspaces between them. The strains of $Li^+$ insertion/extraction were accumulated, resulting in the change of the morphology. Moreover, the poor conductance held back the transfer of electrons, causing a lower rate capability.[35] Furthermore, the SEI films of MGCs are more stable than that of the CMPs. Therefore, as anode materials for lithium ion batteries, $Fe_3O_4$ nanoparticles modified by GSs exhibited good cycling performances and high rate capabilities.

## Conclusions

MGCs were prepared by *in situ* deposition of $Fe^{3+}$ and reducing GO with a microwave heater and a following thermal process. The $Fe_3O_4$ nanoparticles were separate on GSs. MGCs exhibited both improved cycling properties and increased rate capabilities. Such enhanced performances were explained as follows. Firstly, the GSs and the interspaces among $Fe_3O_4$ nanoparticles, which acted as buffers, accommodated the strains of $Li^+$ insertion/extraction. Secondly, the GSs, as electronic conductors, improved the conductance. Thirdly, as buffers, the GSs may also relieve the strain associated with the volume variations during cycles. Our results gave a demonstration that metal-oxides/graphene composites synthesized by a microwave heater could be used as the anode materials of lithium ion batteries with superior cycling and rate performances.

## Acknowledgements

This work was partly supported by the "973" National Key Basic Research Program of China (Grant No. 2007CB310500), Chinese Ministry of Education (Grant No. 705040), and National Natural Science Foundation of China (Grant No. 90606009).

## Notes and references

1 J. Zhang, L. B. Chen, C. C. Li and T. H. Wang, *Appl. Phys. Lett.*, 2008, **93**, 264102.
2 P. G. Bruce, B. Scrosati and J. M. Tarascon, *Angew. Chem., Int. Ed.*, 2008, **47**, 2930.
3 H. L. Zhang, Y. Zhang, X. G. Zhang, F. Li, C. Liu, J. Tan and H. M. Cheng, *Carbon*, 2006, **44**, 2778.
4 S. Han, B. Jang, T. Kim, S. M. Oh and T. Hyeon, *Adv. Funct. Mater.*, 2005, **15**, 1845.
5 C. C. Li, X. M. Yin, L. B. Chen, Q. H. Li and T. H. Wang, *J. Phys. Chem. C*, 2009, **113**, 13438.
6 M. Endo, C. Kim, K. Nishimura, T. Fujino and K. Miyashita, *Carbon*, 2000, **38**, 183.
7 J. Wang, S. Zhong, H. K. Liu and S. X. Dou, *J. Power Sources*, 2003, **113**, 371.
8 M. B. J. G. Freitas, T. R. Penha and S. Sirtoli, *J. Power Sources*, 2007, **163**, 1114.
9 J. Chen, D. H. Bradhurst, S. X. Dou and H. K. Liu, *Electrochim. Acta*, 1998, **44**, 353.
10 M. Venkatraman and J. W. V. Zee, *J. Power Sources*, 2007, **166**, 537.
11 P. Poizot, S. Laruelle, S. Grugeon, L. Dupont and J. M. Tarascon, *Nature*, 2000, **407**, 496.
12 L. B. Chen, N. Lu, C. M. Xu, H. C. Yu and T. H. Wang, *Electrochim. Acta*, 2009, **54**, 4198.
13 Z. M. Cui, L. Y. Jiang, W. G. Song and Y. G. Guo, *Chem. Mater.*, 2009, **21**, 1162.
14 S. Mitra, P. Poizot, A. Finke and J. M. Tarascon, *Adv. Funct. Mater.*, 2006, **16**, 2281.
15 S. Grugeon, S. Laruelle, R. Herrera-Urbina, L. Dupont, P. Poizot and J. M. Tarascon, *J. Electrochem. Soc.*, 2001, **148**, A285.
16 W. M. Zhang, X. L. Wu, J. S. Hu, Y. G. Guo and L. J. Wan, *Adv. Funct. Mater.*, 2008, **18**, 3941.
17 Y. B. Zhang, Y. W. Tan, H. L. Stormer and P. Kim, *Nature*, 2005, **438**, 201.
18 K. S. Novoselov, A. K. Geim, S. V. Morozov, D. Jiang, M. I. Katsnelson, I. V. Grigorieva, S. V. Dubonos and A. A. Firsov, *Nature*, 2005, **438**, 197.
19 J. R. Dahn, T. Zheng, Y. H. Liu and J. S. Xue, *Science*, 1995, **270**, 590.
20 Y. H. Liu, J. S. Xue, T. Zheng and J. R. Dahn, *Carbon*, 1996, **34**, 193.
21 J. F. Shen, Y. Z. Hu, M. Shi, N. Li, H. W. Ma and M. X. Ye, *J. Phys. Chem. C*, 2010, **114**, 1498.
22 X. Y. Yang, X. Y. Zhang, Y. F. Ma, Y. Huang, Y. S. Wang and Y. S. Chen, *J. Mater. Chem.*, 2009, **19**, 2710.
23 H. P. Cong, J. J. He, Y. Lu and S. H. Yu, *Small*, 2009, **6**, 169.
24 H. B. Yin, T. Yamamoto, Y. Wada and S. Yanagida, *Mater. Chem. Phys.*, 2004, **83**, 66.
25 J. A. Gerbec, D. Magana, A. Washington and G. F. Strouse, *J. Am. Chem. Soc.*, 2005, **127**, 15791.
26 N. I. Kovtyukhova, P. J. Ollivier, B. R. Martin, T. E. Mallouk, S. A. Chizhik, E. V. Buzaneva and A. D. Gorchinskiy, *Chem. Mater.*, 1999, **11**, 771.
27 Y. H. Zou, H. B. Liu, L. Yang and Z. Z. Chen, *J. Magn. Magn. Mater.*, 2006, **302**, 343.
28 X. H. Liao, J. M. Zhu, J. J. Zhu, J. Z. Xu and H. Y. Chen, *Chem. Commun.*, 2001, 937.
29 H. Fang, Y. Wu, J. H. Zhao and J. Zhu, *Nanotechnology*, 2006, **17**, 3768.
30 J. S. Zhou, H. H. Song, X. H. Chen, L. J. Zhi, S. B. Yang, J. P. Huo and W. T. Yang, *Chem. Mater.*, 2009, **21**, 2935.
31 Y. T. Lee, J. Park, Y. S. Choi, H. Ryu and H. J. Lee, *J. Phys. Chem. B*, 2002, **106**, 7614.
32 H. Liu, G. X. Wang, J. Z. Wang and D. Wexler, *Electrochem. Commun.*, 2008, **10**, 1879.
33 F. B. Wang, J. Chen, K. L. Huang and S. Q. Liu, *Science China Technological Sciences*, 2009, **52**, 3219.
34 S. M. Paek, E. J. Yoo and I. Honma, *Nano Lett.*, 2009, **9**, 72.
35 Y. S. Hu, Y. G. Guo, R. Dominko, M. Gaberscek, J. Jamik and J. Maier, *Adv. Mater.*, 2007, **19**, 1963.